This is a collaborative proposal; the participating institutions and budget breakdown are as follows:

Institution	yr 1	yr 2	yr 3	yr 4	total
Washington Univ. (Lead)	135,637	132,130	110,090	111,825	489,682
Lamont-Doherty	108,145	102,955	90,336	94,508	395,944
Hawaii	95,249	96,719	100,680	100,311	392,959
Scripps	24,091	41,588	31,808	18,404	115,891
Totals	362,960	373,223	332,736	324,862	1,394,476

1. Introduction and Motivation

The generation and transport of melt beneath oceanic spreading centers is perhaps the most important geological process shaping the earth; it produces over two thirds of the global crust and is a primary means of geochemical differentiation in the Earth. Yet the physical mechanisms controlling melt aggregation, transport, and collection within the axial crust are poorly understood. Most of our understanding of melt dynamics beneath ridges results from petrological and geochemical studies of the materials output by this process. In contrast, the spatial distribution of melt and the associated convective mantle structure have been imaged in few locations. For example, the MELT experiment [e.g. *Forsyth*, 1998] imaged a section across the southern East Pacific Rise (EPR), providing constraints on 2-D subaxial structure. However, both surface morphology and geochemical outputs vary substantially along and between ridge segments so our goal is to take advantage of this fact to understand the relationship between mantle melt processes and the surface manifestation along the ridge. Careful documentation of both crustal and upper mantle structure along a single ridge segment, combined with modeling of mantle flow and melting are required to accomplish this goal. To date, such a 3-D imaging/modeling study has not been attempted along an oceanic spreading center.

The Eastern Lau Spreading Center (ELSC) provides the best location for this work. The ELSC was recently chosen by the RIDGE 2000 (R2K) program for focused, multidisciplinary study, due to its backarc setting and the exceptional along-strike variability in chemistry, petrology, morphology, and hydrothermal flux. Detailed 3-D imaging of the upper mantle and crust will allow us to fulfill the first three of the seven objectives of the Lau Integrated Studies Implementation Plan**: (1) Characterize the mantle flow pattern and the magma production and transport regions; (2) Understand the origin and consequences of gradients in lava composition along the ELSC; (3) Understand the spatial-temporal variations of crustal architecture.**

A combined passive and active seismic experiment along the ELSC will image upper mantle and crustal properties and their along-strike variation over a 250 km long section of the ELSC (Figures 1 and 2) to evaluate the following, previously proposed hypotheses:

1. **Circulation in the mantle wedge is dominated by slab driven flow.**
2. **Interaction of the arc and backarc magma production regions controls the character of the ridge by influencing melt flux, petrology, and geochemistry.**
3. **Variations in the mantle melt supply control ridge crest features such as morphology, thermal structure, and hydrothermal venting.**

The backarc setting of the ELSC provides the ideal opportunity to image along-strike changes in magma production and transport because intermediate and deep earthquakes provide a source array immediately beneath the study area. The energetic, high-frequency signals generated by these nearby earthquakes are essential for successful seismic velocity, attenuation, and anisotropy studies that can be integrated with flow modeling. For example, attenuation tomographic images were readily obtained from the LABATTS backarc deployment [*Roth et al*., 1999] whereas the absence of high frequency body waves prevented such studies for the MELT experiment along the EPR [*W. Wilcock, pers. comm*.].

In order for RIDGE 2000 to achieve its goal of understanding the full mantle-microbe system, an OBS imaging study must be scheduled in the current year. There is a backlog for passive OBSs (first use possible if funded immediately is 2006). Scheduling now will allow the field work to be done in 2006/2007 and the analysis to be nearly complete by the end of the RIDGE 2000 program (2008-2009).

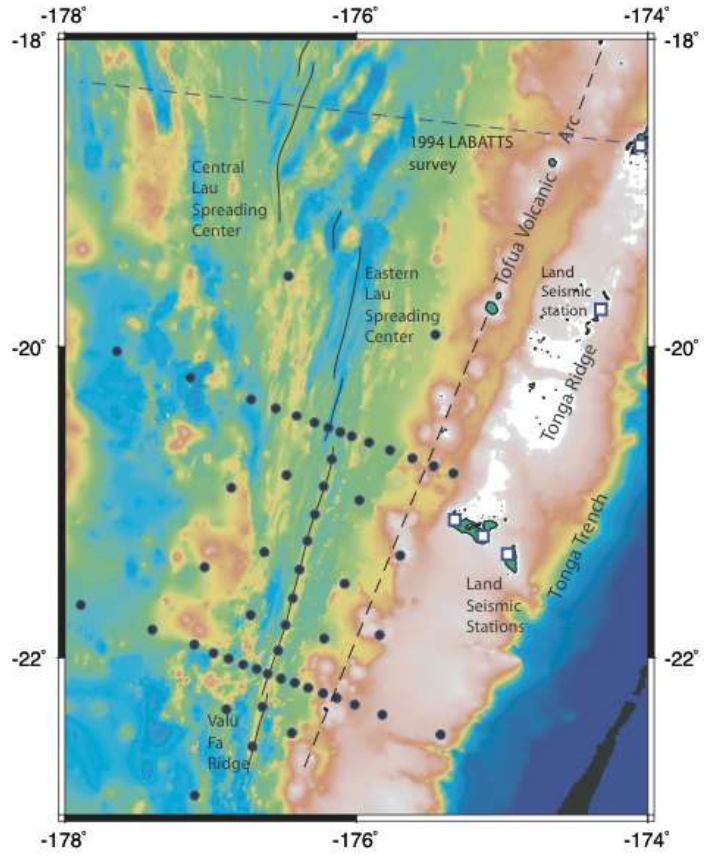

Figure 1 (left): Seafloor bathymetry and layout of the passive-source seismic experiment. Dots indicate OBS positions. Long active-source refraction lines will be carried out along the two long, ridge-perpendicular OBS lines.

Figure 2 (below): (A) Color-shaded bathymetry and layout of the active-source experiment. Triangles represent OBS positions. Shots are fired every ~500 m along the black lines. (B) Northward increase in axial depth and the distance from the ridge to the arc. Blue triangles: hydrothermal vent sites. (C) Spreading rate increases northward, while axial cross-sectional area decreases and axial rise becomes a rift. (D) Mantle Bouguer gravity anomaly increases northward (E) Layer 2A thickness decreases northward. Depth of the AMC reflector is variable. Importantly the reflector is not observed to the north, where the spreading rate is highest. Adapted from Martinez and Taylor [2002] and Jacobs et al., [2003].

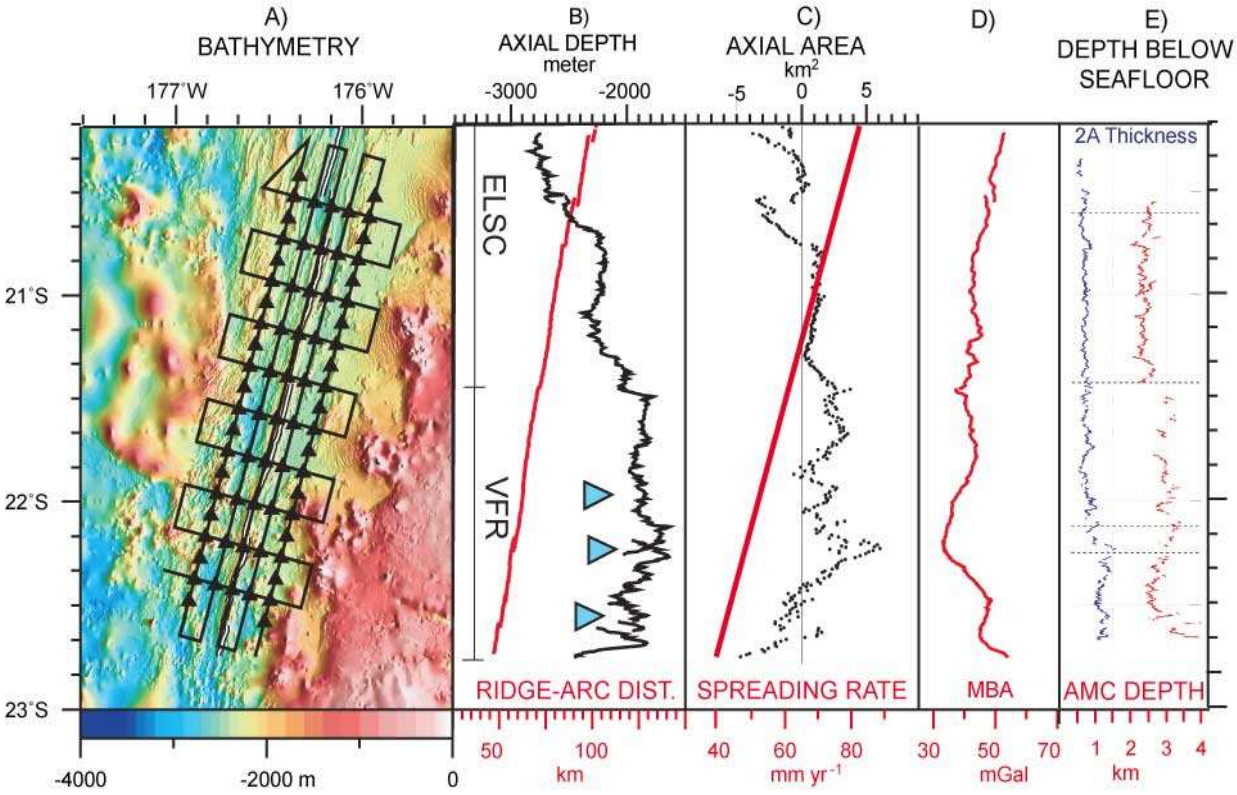

Only two mantle imaging experiments have occurred in backarc settings ñ the LABATTS experiment in the Lau basin (1994) and the Mariana Subduction Factory experiment in 2003-2004. These experiments address problems distinct from those outlined for the ELSC above, and are insufficient to answer the questions addressed in this proposal for the following reasons:

LABATTS (Funded through core MG&G)

1) Imaged the Central Lau Spreading Center (CLSC), characterized by conventional MOR morphology and chemistry: did not cover any part ofELSC, the RIDGE 2000 ISS site
2) Was a 2-D deployment and so provided only sparse information about along-strike changes
3) Had ~50 km OBS spacing, which provided very coarse resolution in the subaxial region
4) Was only a 3 month deployment using narrowband OBSs, many were deployed in the forearc.
5) Lacked an active source component sufficient to image magma collection and transport in the crust and upper several kilometers of the mantle.

MARIANA SUBFAC (Funded through MARGINS)

1) Emphasized arc and forearc imaging in the OBS array design, not the backarc spreading center.
2) Imaged a 60 km section of the spreading center that is only weakly 3-D in character
3) Did not conduct high-density active source work so it is not possible to relate deep structure to shallow properties within the crust.

The Mariana Subfac OBSs will be recovered in May 2004 and the analysis should be largely complete by the time our proposed Lau OBS deployment would occur, June 2006. Lessons learned from the Mariana experiment will be incorporated in the final planning for the ELSC experiment.

2. The Eastern Lau Spreading Center

The ELSC is characterized by rapid along-strike changes in many variables (Figure 2) and thus presents an excellent opportunity to understand the importance of various forcing functions in controlling ridge processes. Going from south to north, the spreading rate increases from 40 to 95 mm/yr [*Zellmer and Taylor*, 2001], the ridge axis changes from inflated to an axial valley [*Martinez and Taylor*, 2002], the melt lens disappears and layer 2A thins [*Collier and Sinha*, 1992; *Harding et al.*, 2000], the crustal composition changes from andesitic to tholeiitic [*Vallier et al.*, 1991; *Peate et al*., 2001], and isotopic values change from Pacific to Indian Ocean mantle domains [*Pearce et al*., 1995]. Furthermore, the depth of the spreading axis increases, the mantle Bouguer gravity values increase, and active hydrothermal venting disappears [*Fouquet et al*., 1991; *Bortnikov et al*., 1993]. The distance of the ridge from the Tonga arc increases from 30 km to 100 km and the depth to the underlying slab increases from 150 km to 250 km.

It is hypothesized that many of the along-strike changes in the ELSC are produced by variable geochemical and petrological inputs via subduction, with the greatest influence in the south where the ridge is closest to the arc [*Martinez and Taylor*, 2002; *Pearce et al.*, 1995]. It is likely that the unusual chemistry observed in Valu Fa hydrothermal vents, particularly the enrichment in Zn and other metals, is related to the enriched andesitic crustal composition and the influence of slab-derived volatiles [*Fouquet et al.*, 1993; *Herzig et al.*, 1993]. Thus, mantle melting processes appear to play a vital role in forming the chemical systems that are fundamental to the Lau vent ecosystems.

Despite the inferences that can be made based on petrology and geochemistry, the physical processes by which the slab de-fluidization may influence the ELSC to produce the systematic morphologic and other signals are currently just (reasonable) conjecture. The missing link is the pattern of flow in the mantle wedge and its relation to variation in melt chemistry, distribution, and migration paths to the ridge.

3. Models of Mantle Processes and Specific Hypotheses to Test

Because of the unique character of the ELSC and the frequent, energetic, and high-frequency earthquake events nearby, the ELSC offers perhaps the best location for revealing the mantle's role in governing ridge crest processes and thus the best opportunity to answer several fundamental questions concerning this interaction. Qualitative and conflicting models of mantle flow and melt supply have

been proposed to explain the observed trends in ELSC characteristics. Here we briefly summarize those models and highlight the testable hypotheses that our study will address.

3.1 Backarc mantle circulation is dominated by slab driven flow

The flow pattern in the mantle wedge of a subduction zone controls many factors, including the location and degree of decompression melting [*Andrews and Sleep*, 1974, *Conder et al*., 2002] and the spatial variation in geochemistry [*Hochstaedter et al*., 2001]. Most modeling studies assume a 2-D geometry and predict that mantle structure will be dominated by slab-driven flow [*McKenzie*, 1979; *Ribe*, 1989; *Davies and Stevenson*, 1992; *Kincaid and Sacks*, 1997]. The long-term (>40 Myr, ODP ë92) Pacific plate subduction, the high convergence rate in comparison with backarc spreading rates, and the great length of the Tonga Trench all lead to a prediction of dominant trench perpendicular flow beneath the Lau Basin. *Martinez and Taylo*r, [2002; 2003] embrace this view in their explanation of the along-strike variation in axial characteristics (Figure 3). They propose that (1) the spatial proximity of the Valu Fa Ridge to the arc causes the ridge to tap arc volcanic melts (slab-hydrated) and receive an enhanced melt supply, (2) mantle wedge return flow of depleted material is responsible for the melt starved tectonics of the Northern ELSC where the ridge is farther from the arc, and (3) farther to the north along CLSC, the ridge is sufficiently far away from the slab, such that it taps "normal" mantle and shows typical MOR characteristics.

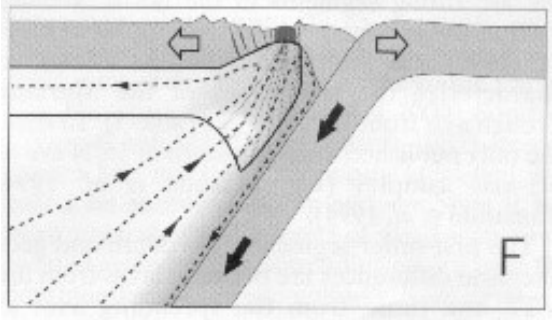

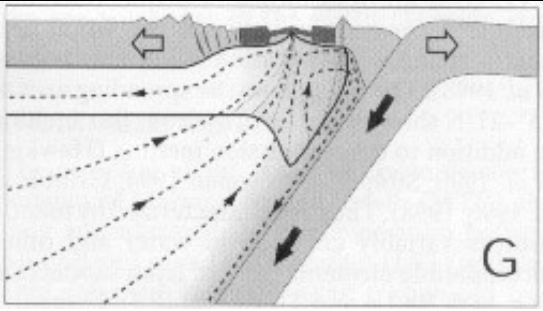

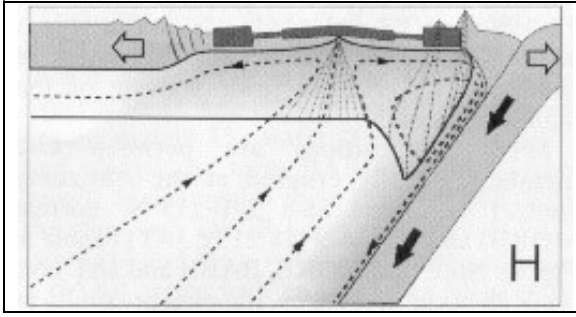

Figure 3: The *Martinez and Taylor* [2003] model for ridge-arc interaction. (Top left) The ridge is close to the arc and "pirates" arc melts. (Top right) The ridge is further from the arc and receives depleted mantle from the arc system, which reduces the melt supply to the ridge. (Lower left) The ridge is sufficiently far from the arc to be uninfluenced by the arc. Flow lines are hypothetical rather than calculated.

Alternatively, 3-D mantle flow may contribute significantly to the observed ridge characteristics. *Turner and Hawkesworth* [1998] suggest that mantle flows in around the northern edge of the subducting plate (Figure 4) since isotopic data from rock samples from the northern Lau Basin show a $^{3}He/^{4}He$ signature distinctive of the Samoan hot spot. *Smith et al*. [2001] infer that observed trench-parallel fast S polarization directions reflect this inflow of Samoan-signature mantle. In addition, slab rollback may occur at a rate up to ~100 mm/yr and could draw asthenosphere into the wedge from around the sides and the bottom of the slab [*Buttles and Olson*, 1998; *Kincaid and Griffiths*, 2003].

We propose to test the 2-D versus 3-D hypothesis by determining the mantle flow pattern in the Lau basin using seismic anisotropy. Various field and laboratory studies [e.g. *Nicolas and Christensen*, 1987; *Mainprice and Silver,* 1993; *Zhang and Karato*, 1995; *Zhang et al.*, 2000;] confirm that deformation-induced mineral orientation produces a 'fast direction' of upper mantle anisotropy aligned close to or along the flow direction. Thus, the fast S-wave polarization and fast P-wave propagation directions should be dominantly trench-perpendicular if the 2-D hypothesis is true. Subduction-dominated flow in

the mantle wedge should also produce notable asymmetry in the distribution of melt beneath the backarc spreading center [*Conder et al.,* 2002]. Detailed shear wave splitting and surface wave anisotropy measurements throughout our passive OBS array will go far beyond the currently available, sparse splitting data for the Lau mantle wedge farther to the north. Station coverage every several kilometers will be critical to deduce any variation in anisotropic signature. If fast polarization directions beneath the eastern basin are consistently trench-parallel, the 2-D flow hypothesis can be ruled out. For a 3-D flow scenario, the pattern of anisotropy must vary in a manner that can be tied to a reasonable velocity field and be consistent with temperature and melt distributions inferred from the other seismic and geochemical results.

Some recent experiments suggest a different relationship between the 'fast direction' of anisotropy and flow, either due to the presence of water [*Jung and Karato*, 2001] or through melt segregation into weak shear zones [*Holtzman et al*., 2003]. If such results are applicable in the Lau mantle wedge, it would likely only be in limited areas: adjacent to the slab (high local fluid content), or within migration 'channels' where fluid/melt occurs at fairly high fraction. Rapid spatial variability in anisotropic signals could help us recognize such regions, if they exist.

3.2 Spatial relation between arc and backarc melt production regions controls ridge characteristics

Slower spreading ridges usually exhibit median valleys and faster ridges exhibit axial highs [*Malinverno*, 1993; *Small,* 1998], with the differences thought to arise because of the different thermal structures [*Phipps Morgan et al.,* 1987; *Phipps Morgan and Chen*, 1993; *Shah and Buck*, 2001] and the amount of inflation from magma supply [*Scheirer and Macdonald*, 1993]. However, the ELSC shows the opposite pattern, with ridge inflation towards the slower spreading southern end and median valley features toward the faster spreading northern end. As the spreading rate along the ELSC decreases to the south, the ridge becomes steadily closer to the arc and, petrological and geochemical measurements reveal arc influences on ELSC magmas, with high Ba/La and low Na, Ti, and Fe. These trends imply enhanced upper mantle melting due to fluid enrichment from the slab [*Stolper and Newman*, 1994; *Taylor and Martinez,* 2003]. The ELSC also shows enrichment in other fluid mobile elements [*Hawkins,* 1976; *Pearce et al.*, 1995], therefore fluids must be transferred from the slab to the melt production region of the spreading center by some physical process. This gradient in slab fluid influence to the south led *Martinez and Taylor* [2002] to speculate that the ridge taps melt from the arc magma region when the proximity reaches a given threshold resulting in an axial high.

While this ëmagma piracyí model [*Martinez and Taylor*, 2002] appears to be a viable mechanism to explain ELSC chemistry and morphology, 3-D effects from the nearby termination of the spreading axis, trench-parallel asthenospheric flow in the wedge, or even variable mantle viscosity could significantly alter the upwelling pattern and thermal structure and in turn govern the ridge morphology and melt chemistry. The "piracy" model also assumes that the subaxial melt generation region is wide and will therefore begin to interact with the arc melt generation region when ridge-arc separation drops below ~100 km. While passive upwelling at the ridge would likely produce such a broad melt region, melt generation via buoyancy-enhanced upwelling may concentrate low-density melt into a narrow, low-viscosity channel beneath the axis [e.g., *Buck and Su*, 1989]. In this case the subaxial melt region beneath the ELSC would be too narrow to directly interact with arc melts.

These two end-member models, broad or narrow upwelling, predict different seismic signatures in both velocity [*Forsyth et al*., 1998] and anisotropy [*Blackman et al*., 1996; 2002b]. The LABATTS and MELT experiments measured seismic anomalies beneath the fast-spreading CLSC and the EPR that are consistent with a broad zone of upwelling and melt production [*Zhao et al*., 1997; *Forsyth et al., 1998*; *Toomey et al., 1998*; *Hung et al*., 2000; *Dunn and Forsyth*, 2003]. However, upwelling may develop into 3-D structures beneath ridges with slow spreading rates and/or low mantle viscosity [*Parmentier and Phipps Morgan*, 1990; *Magde and Sparks*, 1997; *Niu et al*., 2001]. Mantle viscosity could be low beneath the ELSC due to fluxing of slab fluids [*Hirth and Kohlstedt*, 1996] and regionally hot temperatures [*Kelley et al*., 2003; *Taylor and Martinez*, 2003]. Coupled with a fairly slow spreading rate, this makes the ELSC a far better candidate for buoyancy-enhanced upwelling than either of the other RIDGE2000

integrated study sites. Because the ELSC spans a crucial transition in seafloor roughness that is interpreted to accompany changes in melt flux [*Small and Sandwell*, 1992; *Ma and Cochran*, 1997], it is an excellent place to test both whether the ridge taps arc melts at depth and whether there is any 3-D upwelling pattern.

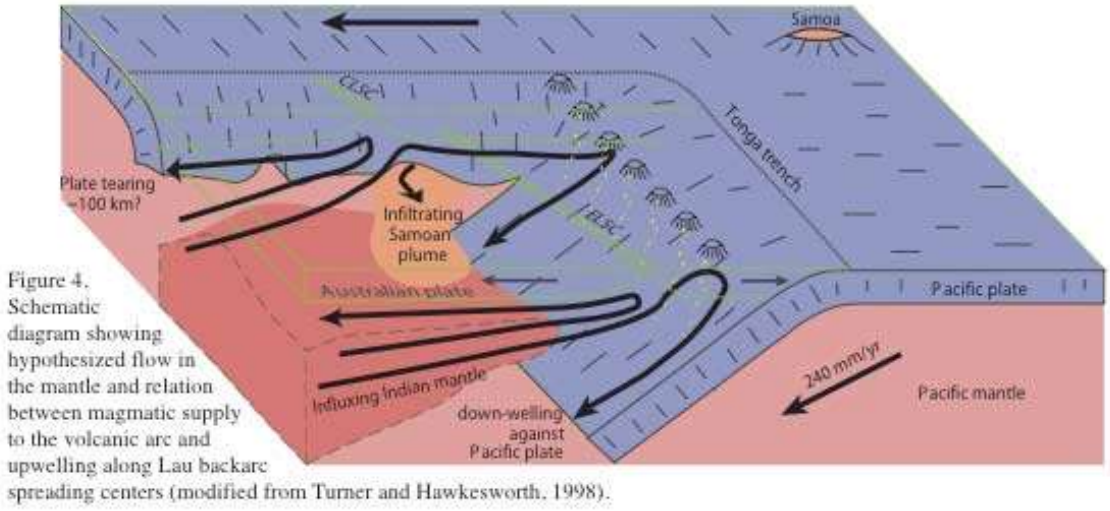

Figure 4. Schematic diagram showing hypothesized flow in the mantle and relation between magmatic supply to the volcanic arc and upwelling along Lau backarc spreading centers (modified from Turner and Hawkesworth, 1998).

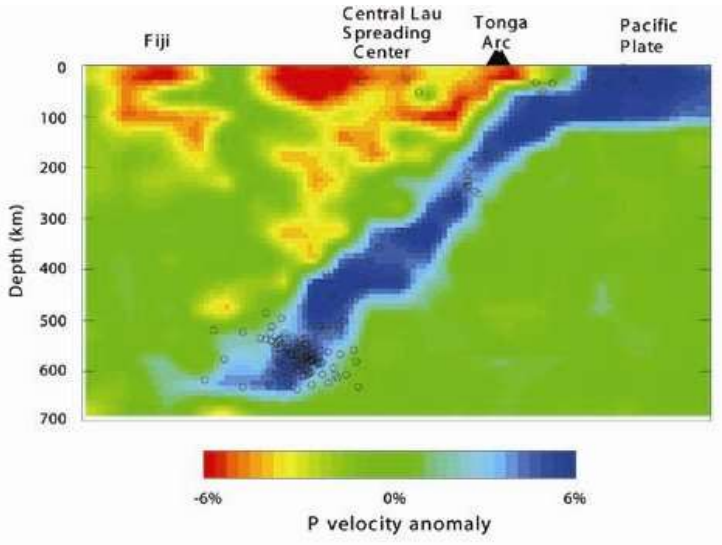

Figure 5. P-wave tomography of the Tonga subduction zone and Lau backarc obtained from the LABATTS deployment [Zhao et al., 1997]. Low P wave velocities delineate the magma production zones of the Tonga arc and Central Lau spreading Center. Circles show seismic sources. The proposed experiment has a smaller station spacing, a 3-D layout, and will result in a much higher resolution 3-D image of structure along the ELSC, the R2K IS site.

We propose to determine the degree of spatial interaction between arc and backarc spreading center magma production regions using P, S, and attenuation tomography. The presence of melt can be distinguished by large Vp/Vs ratios and from the magnitude of the velocity anomalies [*Hammond and Humphreys,* 2000a]. 3-D tomography will delineate variations in the along-strike shape and extent of the subaxial melt and delineate arc-backarc connections in melt supply and variations of that connectivity along strike. For example, much lower resolution P-wave tomography from the LABATTS experiment (figure 5) shows separate shallow magma production regions for the CLSC and the Tonga arc, consistent with the lack of subduction influence along the CLSC. If the ELSC taps magma from the arc source region, this should be observable in the tomography with a slow Vp, but high Vp/Vs region extending deeper beneath the axis and possibly eastward to reflect the connection with the arc magmas. It is not clear whether the ìmagma piracyî would occur through actual entrainment of arc

magmas or simply through enhanced melting and trace element transfer via slab released water. It may be possible to seismically differentiate these models using the combined observations of attenuation, Vp, Vs, and dlnVs/dlnVp [*Wiens and Smith*, 2003] as well as future experimental work on the effect of fluids on mantle seismic properties.

3.3 Variations in the mantle melt supply control ridge crest features such as morphology, thermal structure, and hydrothermal venting.

A fundamental hypothesis is that the strongly varying character of the ELSC, as shown in Figure 2, is controlled by spatial variations in mantle melt flux and crustal melt storage beneath the ridge. Yet to date, mantle melt flux and the crustal and sub-crustal accumulation of melt are very poorly known.

Questions related to the above hypothesis include: *What controls the cross-sectional area of an axial rise?* The degree of axial inflation is inferred to reflect magma storage and hence supply [*Scheirer and Macdonald*, 1993], yet may just reflect flexural effects due to thermal structure and cooling [*Eberle and Forsyth*, 1998a,b, *Shah and Buck*, 2001]. *What controls the formation of an axial rift versus an axial rise*? These large differences in ridge morphology are interpreted to be due to spreading-rate controlled differences in thermal structures [*Phipps Morgan et al*., 1987; *Phipps Morgan and Chen*, 1993; *Eberle and Forsyth*, 1998a,b, *Shah and Buck*, 2001], yet existing models are conflicted in the mechanism that supports an axial high due to a lack of knowledge of a ridge's thermal structure for a rift versus a rise. *What controls the morphologic segmentation of the ridge?* Overlapping and non-overlapping offsets occur along the ELSC, such as near 20˚50'S, ~21˚20'S, and 22˚15'S. Along the EPR the apparent volcanic segmentation of the ridge [*Haymon et al*., 1991; *Langmuir et al*., 1986] has been correlated with variations in mantle melt supply [*Dunn et al*., 2000, 2001], whereas larger overlapping offsets may be due to tectonic stresses [*Lonsdale*, 1983; 1989; *Dunn et al*., 2001]. *Is enhanced hydrothermal activity correlated with enhanced melt supply along the Valu Fa Ridge?* Enhanced hydrothermal output is often attributed to higher melt flux, yet hydrothermal systems vary on short time scales and may not reflect mantle melt flux differences or even crustal melt storage differences. Unfortunately, space does not permit a more thorough discussion of these and other important questions.

The best indicator of the integrated melt flux over time is crustal thickness and arguably the best way to determine crustal thickness is through a wide-angle refraction/reflection experiment. Furthermore, the highest resolution constraints on melt content in the crust and sub-Moho mantle are currently determined via high-resolution tomographic imaging [e.g., *Dunn et al*., 2000; 2001] (except for detailed images of melt storage in the shallow melt lens obtained via MCS studies). Our proposed active-source experiment, discussed below, has been carefully designed to image crustal thickness, thermal structure, and melt content along the ELSC and to test the above hypothesis and answer its related questions. The experiment will provide detailed images of the RIDGE2000 study site "bulls-eye" and images to the north and south for direct comparison. The experiment is co-located with the passive-source experiment and provides a crucial view of the connection between the near surface processes and the deeper mantle.

4. Proposed Data Collection

4.1 Passive broad-band survey and ridge crest microearthquake monitoring

The goals of the passive experiment (Figure 1) are to:

1) *Provide 3-D body wave P, S, and attenuation tomographic images of the entire ELSC and Tonga volcanic arc,* with enhanced resolution near the ìbullseyeî for R2K studies and at another ìmagma starvedî location farther to the north.

2) Map the variation in mantle flow, as indicated by seismic anisotropy within the Lau mantle wedge. Seismic anisotropy will be determined from shear wave splitting studies and from tomographic imaging using surface waves traversing the array.

3) Map seismicity along the ridge crest to investigate ridge crest tectonic processes. Earthquake locations and mechanisms will provide constraints on tectonic processes and earthquake depths will help constrain thermal structure.

To achieve these goals we have designed an array of 55 OBSs that features two long, cross-axis lines with closely spaced instruments within a larger, more widely spaced grid. One of the lines will be centered on the location of the RIDGE2000 ISS ìbullís-eyeî. The ìbullís-eyeî is not yet determined (see the Lau ISS Implementation plan on the RIDGE2000 web site), but will be determined in 2005 and is likely to be near the known hydrothermal sites around 22ºS. The northern dense line of the passive survey is designed to examine structure along the "magma starved" section of the ELSC and provide direct comparison to the more "robust" but slower spreading southern section. The surrounding grid of OBSs is necessary to accurately locate earthquakes within the subducting slab, fill in the three dimensional tomographic map of the area, and map out variations of anisotropy. The body wave tomography will be inherently 3-D due to the distribution of earthquake sources, but resolution will be enhanced along the two dense lines. Instrument concentrations near the ìbullseyeî and near the intersection of the northern line with the ridge crest will be sufficient to resolve microearthquake depths and locations to reasonable precision ($\pm$ 500 m in location, $\pm$ 1 km in depth).

The Tonga trench is the most seismically active region in the world, accounting for one quarter of the intermediate and deep events worldwide. We expect to easily obtain sufficient slab earthquakes for the passive tomography within the ten-month period, based on our experience with the previous experiment. Note that ocean bottom seismometers have improved greatly since the LABATTS experiment a decade ago, which was the first large experiment that used OBSs to study structure within the mantle. The new OBSIP instruments have a much longer recording duration, lower noise levels on all three components [e.g., *Webb et al*., 2001], and wider dynamic range (24 bit instead of 16 bits) thus eliminating the problem of clipping for large events.

The OBS array will be augmented with five land broadband seismic stations on the adjacent Tongan islands to increase the aperture of the array and to better locate small earthquakes necessary for tomography at lower cost compared with installing further OBSs. These stations will be obtained from the PASSCAL instrument center and will be installed and operated by Wiens, Conder, and Wash. Univ. technical scientist Patrick Shore. All three have extensive experience installing and operating stations in Tonga, and have a good working relationship with Tongan government officials.

4.2 Active Survey ñ Goals and Data Collection

One of our principle scientific objectives is to determine how variations in ridge crest structure and processes may be related to variations in the underlying mantle melt supply and crustal melt accumulation. To achieve this objective we will:

1) Map the seismic velocity structure of the uppermost mantle beneath a 250-km-long section of the spreading center. By undershooting the spreading center with mantle *Pn* waves, we will image the mantle velocity structure just beneath the crust-mantle interface to determine whether melt content is relatively uniform or varies along the ridge. To first order, we will also measure the orientation and magnitude of anisotropy in the uppermost mantle and estimate the general mantle flow direction.

2) Image the seismic velocity structure of the crust along this 250-km-long section of the ELSC. A series of ridge-perpendicular seismic profiles spaced 24 km apart will image crustal melt storage and the ridge thermal structure with crustal refractions and wide-angle Moho reflections. This includes for a section of rifted ridge near 20˚30'S and the section of rise along the Valu Fa, and thus provides strong constraints for models of melt supply and rift/rise formation. Two high-resolution, ridge-parallel seismic lines will image 250-km-long 2-D sections of the crust and uppermost mantle located 20 km to either side of the ridge. We will also image spatial variations in crustal structure between these high-resolution profiles using seismic energy that crosses between these lines.

3) Construct a map of crustal thickness variations along and across the spreading center. Wide-angle reflections off the mantle will be recorded throughout the 250x40 km region of the experiment and provide a map of crustal thickness variations throughout the region. Competing magma supply models can be critically evaluated by correlating crustal thickness with other indicators of magma supply. In addition, a crustal thickness map is necessary to remove the effects of crustal thickness on the mantle-imaging portion of this experiment. Crustal structure and thickness measured along two long ridge-

perpendicular transects (Figure 1) will reveal the history of crustal accretion and hence melt flux for a section of ridge with a rifted character versus a section with a rise.

The experiment consists of a grid of OBSs extending 250 km along the ELSC with a station spacing of 10-12 km (Figure 2a); airgun shots will occur along ridge parallel and perpendicular lines. We will use the same instrument and shot spacing as for the EPR UNDERSHOOT experiment except with additional stations nearer the rise and more cross-axis shot lines for imaging the crust and obtaining better azimuthal coverage in the mantle (see Results from Prior for R. Dunn). Additional shots will occur along the two long ridge-perpendicular transects (Figure 1). On the basis of our experience with previous 3-D tomography and undershooting studies [*Dunn et al*., 2000; *Dunn et al*., 2001; *Christopher et al*., 2003; *Dunn et al*., 2003] and preliminary resolution tests (Figures 6-7), the proposed geometry will provide a dense coverage of intersecting ray paths from a broad range of angles that will allow us to image 3-D structure on a scale of 1-3 km in the crust (smaller values along the 2-D transects) and 2-4 km at upper mantle depth.

5. Data Analysis

Our team has extensive experience successfully carrying out active-source and passive-source seismic experiments and analyses and the modeling proposed here (see Prior Support section). In this section we summarize some of those methods that we will apply to the data.

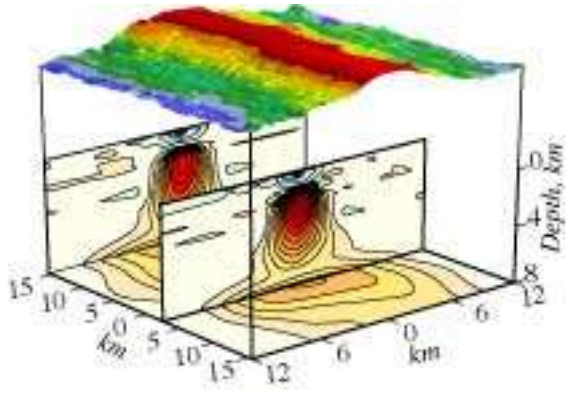

Figure 6: Our experiment will obtain profile and planar-layer images of the crust and upper mantle with higher resolution than this P-wave velocity image from the EPR near 9˚30'N. [Dunn et al., 2000]. Velocity perturbations (with respect to a 1-D model) are contoured at 0.2 km/s intervals.

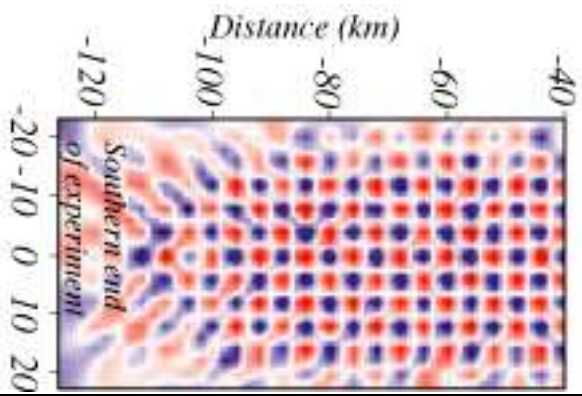

Figure 7: Checkerboard resolution map of a planar layer in the uppermost mantle, 8 km depth, illustrates the high resolving power of the proposed experiment geometry. For clarity we only show the southern 85 km portion of the total mantle plane.

5.1 Active Survey ñ Data Analysis

We will construct tomographic images of the crust and uppermost mantle using a new method [*Dunn et al*., 2003] that solves for 2- or 3-D velocity structure, reflector (Moho) topography, and the magnitude and orientation of seismic anisotropy (hexagonal symmetry system). We will use crustal refraction data to test for shallow, crack-induced anisotropy due to lithospheric stretching [e.g., *Dunn and Toomey*, 2001; *Barclay et al*. 1998] and mantle *Pn* data to constrain the magnitude and azimuth of uppermost mantle anisotropy [e.g., *Dunn et al*., 1997; *Dunn et al*., 2001]. We will quantitatively examine any trade-offs between isotropic velocity, crustal thickness, and anisotropy. The velocity images will be analyzed using theoretical and experimentally derived relations for the effects of temperature and melt fraction on seismic velocity to constrain the thermal structure and melt distribution beneath the spreading center. We will integrate our results with the deeper mantle seismic images and other indicators of melt supply to develop an integrated model of melt flux from its point of origin, up through the mantle, and into the crustal storage reservoirs and to determine the origin of the large variations in ridge character.

5.2 Passive Body Wave Tomography

The dataset of P and S arrivals will be inverted using iterative 3-D tomographic methods. Crustal structure determined from the active source part of this experiment will be incorporated as *a priori* information. Rays will be retraced and local earthquakes relocated in the 3-D structure between iterations for the structure model. We expect to use inversion methods that solve for the P structure and the P/S anomaly ratio [*Conder and Wiens*, 2003]. Inter-station spacing ranges from 10-30 km in the region of study, so a resolution on the order of 25 km should be obtainable.

P velocity, *S* velocity, and attenuation are each sensitive to the temperature, melt content, composition, and fluid content in different ways [*Roth et al.*, 2000; *Wiens and Smith*, 2003]. Attenuation has an exponential dependence on temperature [*Jackson et al.*, 1992] while velocity has a largely linear dependence. Also, attenuation is largely insensitive to melt content [*Hammond and Humphreys*, 2000b], so attenuation tomography (although of lower resolution) furnishes independent information on material properties [*Roth et al.*, 2000]. Therefore, the best constraints on material properties result from the simultaneous interpretation of all three observables. Determining the *P, S*, and attenuation structure with tomographic methods will be key to understanding the structure of the mantle wedge and sub-ridge upwelling zone. 3-D *P* and *S* wave tomography will be performed using both regional and teleseismic arrivals. We estimate that about 1500 well-located regional earthquakes will be recorded during the ten-month deployment within 400 km of the array, which should provide about 50,000 arrival times at the OBS array.

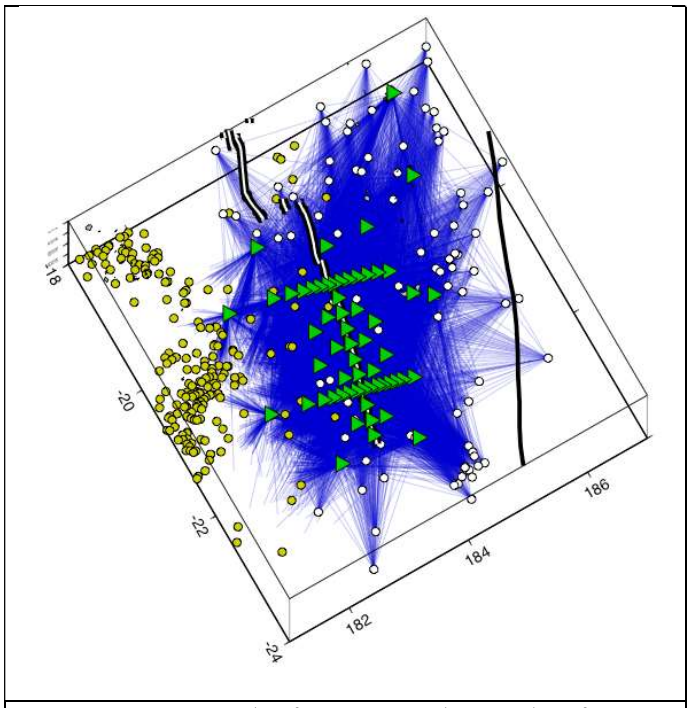

Figure 8. Ray paths for a 9-month sample of Tonga earthquakes recorded by the global network. Green triangles show proposed OBS array, straddling the ELSC; black line marks trench; white/yellow circles show shallow/intermediate depth earthquakes. Many additional slab earthquakes will be detected by the OBS array so the total events available for tomography will be much greater than is shown here. Paths for teleseismic earthquakes (not shown) will also increase coverage.

5.3 Body wave analyses & seismic anisotropy

To test models of strain & fabric development associated with flow in the mantle, we will measure the pattern of shear wave splitting times and apparent fast (P- and S-polarization) directions. Techniques for measuring split shear waves in regions of simple azimuthal anisotropy are well developed [e.g. *Savage*, 1999, *Wolfe and Silver,* 1998; *Smith et al*., 2001]. Of special interest for this study, however, is determining whether the data require more complex patterns of anisotropy, such as are expected to accompany 3-D flow [e.g. *Hall et al*., 2000; *Blackman and Kendall*, 2002] that could bias interpretations based on simple assumptions [e.g. *Chevrot and van der Hilst*, 2003; *Schulte-Pelkum and Blackman*, 2003]. We will apply a newly developed data analysis method [*Menke and Levin,* 2003] to assess the statistical significance of more complex scenarios. OBS orientations can be determined using well-located earthquakes with an accuracy of ±5∞RMS [*Hung et al*., 2000] so this is the precision for the anisotropy orientations. Surface wave analyses (see next section) will also help constrain anisotropy, particularly its vertical distribution.

The anisotropy results will be evaluated using flow modeling, texture estimates and synthetic seismogram calculations. We will develop a series of flow models in which relevant parameters are varied (e.g. viscosity, melting curves, effect of water, amount of along-trench flow) using temperature dependent viscosity [e.g. *Conder et al*., 2002]. Both finite strain and poly-crystal plasticity methods will then be used to estimate the mineral texturing (lattice preferred orientation); corresponding anisotropic elastic constants will be computed, and the seismic response of each model will be estimated using Menke's SPLITTING-MODELLER code.

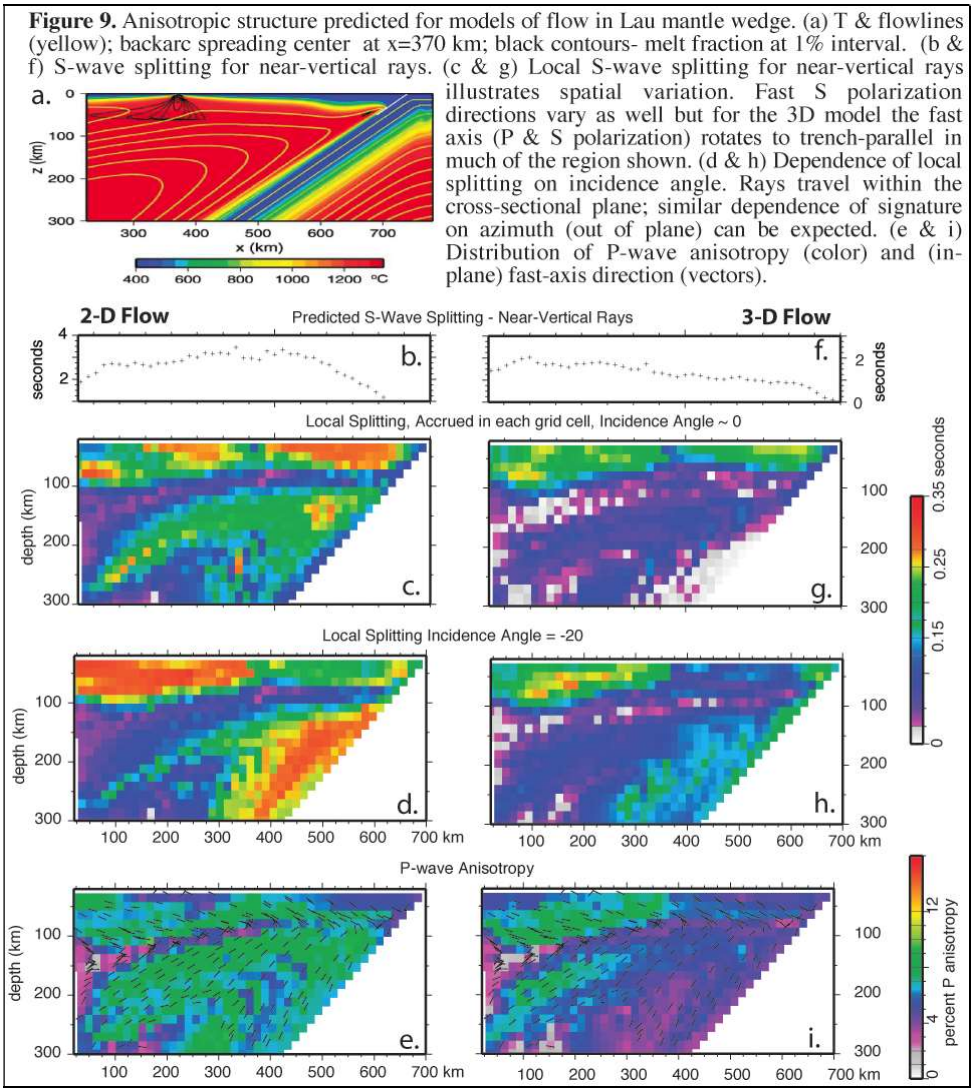

Figure 9. Anisotropic structure predicted for models of flow in Lau mantle wedge. (a) T & flowlines (yellow); backarc spreading center at x=370 km; black contours- melt fraction at 1% interval. (b & f) S-wave splitting for near-vertical rays. (c & g) Local S-wave splitting for near-vertical rays illustrates spatial variation. Fast S polarization directions vary as well but for the 3D model the fast axis (P & S polarization) rotates to trench-parallel in much of the region shown. (d & h) Dependence of local splitting on incidence angle. Rays travel within the cross-sectional plane; similar dependence of signature on azimuth (out of plane) can be expected. (e & i) Distribution of P-wave anisotropy (color) and (in-plane) fast-axis direction (vectors).

Figure 9 illustrates how anisotropy developed during 2-D flow might differ from that for 3-D mantle flow. A component of along-trench velocity is added to the 2-D Conder et al. (2002) model. A gradient in the along-strike flow is assumed, higher in the north and reduced toward the south, to simulate influx of Samoan plume material. The magnitude of the along-strike gradient is about 1/3 the maximum gradient in the 2-D flow field. Linked numerical calculations (*Blackman et al*., 2002a) of evolution in olivine:enstatite grain orientations along flowlines and corresponding effective elastic constants give local P anisotropy and S splitting. Since the velocity gradients vary throughout the flow field, the anisotropy also varies as the strength and orientation of the texture evolves. Changes in polarization direction of the fast S-wave also vary but much of the model space is characterized by rotation from trench-perpendicular (2D) to trench-parallel (3D), for near-vertical incident rays. Near the plates that drive the (2D) flow, shallower rays show more rotation than steep rays.

Interpretation and modeling of anisotropy in the vicinity of plate boundaries is quite challenging; we approach this portion of the project with a good understanding of the strengths and limitations of the methods. Our plan is to conduct the data analysis hand in hand with preliminary modeling. Integration of P, S, and surface wave data will consume a good portion of our efforts. Possible next steps might include: 1) adding the effect of texturing on the resulting flow field [*Christensen*, 1984]; 2) adding the effect of melt on anisotropy [*Schmeling*, 1985; *Faul et al*., 1994; *Kendall*, 1994; *Holtzman et al.,* 2003]. 3) adding the effect of water on olivine alignment during flow [*Jung and Karato*, 2001]; a shift between dominant glide systems, keyed to environmental parameters of the flow field, can be incorporated in our method. In any case, our modeling will be guided by observed pattern of anisotropy.

5.4 Surface wave Analysis

Surface wave observations provide a robust means of mapping the shear velocity structure in the upper mantle beneath the ELSC. We expect to detect along-axis variations in lithospheric thickness and in the width and depth extent of the low-velocity zone associated with varying melt fractions and temperatures beneath the ridge and above the subducting slab. Anisotropy constraints determined by combining Love and Rayleigh wave observations are particularly important in constraining the depth of anisotropy, since most body wave methods such as SKS splitting provide poor depth constraint. OBSs now routinely produce good signal to noise ratio for Rayleigh waves at periods from 10 to 100s, [*Weeraratne et al.,* 2003] and for Love waves from 5 to 20s [*Dunn and Forsyth,* 2003], constraining structure in the uppermost 150km for Rayleigh waves and uppermost 50-70km for Love waves. We will combine two techniques: surface wave tomographic inversion applied to data from teleseismic events, and the new method of *Dunn and Forsyth,* [2003] applied to short period Love and Rayleigh wave records from regional events.

Phase velocities determined from analysis of surface waves from teleseismic events will provide constraints on the larger scale and deeper structure. We will use one of several sophisticated methods for inverting surface wave data collected with arrays have been developed in recent years [*Friedrich*, 1998; *Forsyth et al*, 1998; *Laske et al*., 1999]. In general these methods involve solving for the back azimuth of the incoming wavefront as a function of frequency, some methods allow for multiple plane waves to correct for multipathing before determining the frequency-dependent inter-station phase velocities. An azimuthal dependence to the phase velocities indicates azimuthal anisotropy.

We will also use the method of *Dunn and Forsyth* [2003] to model short-period Love and Rayleigh waveforms of 0.02-0.2 Hz (<0.07 Hz for Rayleigh waves due to water column interference). With sufficient station density, as proposed here, this method actually exploits the waveform complexities from multi-pathing to strongly constrain details of mantle structure at scales of 10 to 20km (figure 10). The method models group, phase, and amplitude variations across the array, which are sensitive indicators of velocity variations beneath the ridge. A new version of this method allows for three-dimensional solutions. Ray paths that arrive from a wide range of azimuths will reveal both across- and along-axis variations in asthenospheric and lithospheric structure.

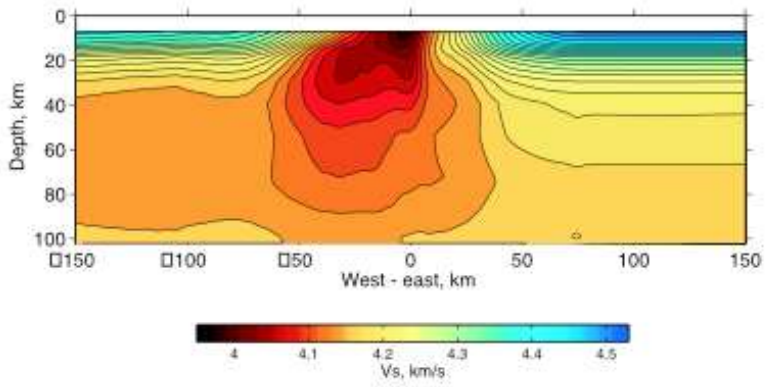

Figure 10. Shear velocity image of the southern EPR illustrating the resolution attainable for imaging lithospheric thickness and the upwelling zone using short-period surface waves. (Ridge axis located at x=0 km; image is oriented perpendicular to the ridge.) Importantly, sharp variations in velocity structure on the 10-20 km scale can be resolved with this method. (Compare with Figure 5 and note the difference in size of regions imaged.)

5.5 Local Seismicity

The ten-month passive array deployment will provide one of the best records of seismicity along a ridge segment yet obtained by any experiment. The inter-element spacing (12-15 km) near the axis is sufficient to accurately (<0.5km) locate all significant tectonic events along the segment. The spreading rates seen along the ELSC (40-90 mm/yr) reflect a range of rates between slow and intermediate ridges. Large events are rare on fast spreading ridges because much of the crust is too hot to exhibit brittle behavior whereas large tectonic events are common at slow ridges. Several studies suggests a systematic variation in the style of faulting [*Shaw and Lin*, 1993] and depth of events beneath slow-spreading ridge segments with deeper events found near the colder ends of segments [eg. *Toomey et al*., 1985; *Kong et al*., 1992] although not all such studies show this trend [e.g., *Wolfe et al*., 1995]. Along the ELSC ridge the apparent magmatic robustness of the southern section would suggest a hotter thermal structure and shallow events. Some earthquakes from the ELSC have been detected at land seismic stations in Tonga.

Earthquakes will be located first using a simple 1-D velocity model with hypocenter estimates further improved by tracing rays through the 3-D model from the tomographic refraction experiment [eg. *Sohn et al*., 2004]. Where possible we will use cross correlation techniques to improve hypocentral (relative location) accuracies [e.g., *Golden et al*., 2003 *Sohn et al.*, 1998]. Focal mechanisms for the larger events would be determined using both P-wave and S-wave arrivals and amplitude ratios [*Shen et al.,* 1997].

The array could provide a clear record of dike propagation should we be fortunate enough to see such a volcanic event during the array deployment. We know of a proposal to deploy hydrophone arrays in the Lau Basin. The hydrophone array would provide accurately locations of shallow events, with small T-wave source region, throughout the Lau Basin, but would provide little constraint on focal depth, and none on earthquake mechanism. The OBS array would provide significant ground truthing of the hydrophone-based results and allow a calibration of earthquake moment versus amplitude at the hydrophones if deployed simultaneously.

Cruise Plan: Deployment Leg	
Leave Nukuíalofa for 1st OBS site	0.5 d
Deploy 55 OBSs for southern half of active source array:	6.5 d
Southern Refraction lines	8 d
Recover 26 OBS and redeploy for northern lines	9 d
Shoot northern lines	6 d
Recover 19 OBSs and redeploy to fill out passive array	7 d
Shoot southern refraction line	1.5 d
Return Nukuíalofa:	0.5 d
Total	39 d

6. Logistics and Work Plan

Combining the active and passive experiments into one set of cruises minimizes costs by 1) using two legs instead of 3 or 4 and 2) using the same OBSs for both arrays avoiding a duplication of costs for ship time, instrument preparation, personnel, expendables (batteries) and shipping. The closest port to the study site is Nukuíalofoa, Tonga. This small port has container ship service. We require the R/V Ewing (or its replacement) during the first leg, which will require 39 days of shiptime (Table 1). Any large ship will be suitable for the 15 day recovery leg that will follow the first by ten months

The active experiment consists of one large central corridor and two long refraction lines. We will shoot to OBSs at 90 locations along about 1900 km of refraction lines. To accomplish this with 55 OBSs we will split the main array into overlapping northern and southern segments and shoot these, and the southern cross-axis line separately. Shots will be spaced 2.5 minutes apart (about 500m at 4.5 kts). There is voluminous evidence that the best refraction data is obtained when water column reverberations are allowed to dissipate between shots. Our plan shifts OBSs between sites in three steps. We use many common sites between the passive and active arrays to minimize the number of OBSs moved. The experiment will require 100 deployments of OBSs, so that 45 OBSs will need to be redeployed during leg 1. We will shift sampling rates from 125 Hz for the active source work to 40 Hz for the passive experiment. We used current OBSIP guidelines for deployment times and a ship speed of 10 knts to calculate the time required for OBS operations. The pickup cruise will occur about 10 months following the deployment and is budgeted in the 2nd grant year. The data will be entered in databases during the 2nd year. The active source experiment airgun lines are restricted to deep water (>2000m). Recent Ewing

airgun source measurements show that in deep water, source levels fall very quickly with range and this is expected to minimize the potential impact of the airguns on marine mammals. So although whales are present in Lau basin, we expect it should be possible to obtain the necessary permits for the cruise. During the cruise, we will follow established rules and guidelines for the protection of marine mammals.

Division of Tasks Amongst Collaborators.

Washington University: Doug Wiens will coordinate the passive part of the experiment, and will take the lead on the body and surface wave tomographic analysis and deployment of the land stations in Tonga. James Conder will develop mantle flow and melting models for comparison with anisotropy and tomographic results and will assist on the body wave tomography. **University of Hawaii:** Rob Dunn will take the lead on the active source part of the experiment and he will supervise the active source data analysis. He will also lead the analysis of short-period surface waves. **LDEO:** Spahr Webb and Bill Menke will take the lead on orienting the OBSs and performing the body wave anisotropy analyses. Webb will interface with the OBSIP on OBS technical issues. LDEO will work with Washington University on the body wave and surface wave tomography. LDEO will collaborate with Blackman to model wave propagation in predicted anisotropic structure for a few flow/texture models. LDEO will work on ridge crest seismicity. **Scripps:** Donna Blackman will coordinate flow modeling with James Conder and work with LDEO to incorporate anisotropy observations into textural modeling. Elastic constants will be predicted for inclusion in wave propagation models for comparison with the data.

7. Broader Impacts

This project will make valuable contributions to scientific infrastructure. New seismic imaging methods and models will be developed and ultimately distributed for use by the community via publication and PI websites. The data sets we collect are substantive and will become part of the R2K Integrated Study Site database that is available to the broader community and will provide productive research in many areas for years to come. Both the land station data and OBS data will be made available through the IRIS data management center. The proposed research is intended to play an important role in accomplishing the goals of the RIDGE2000 science program. RIDGE2000 is a NSF-funded program whose mandate is to focus funds and expertise on the interdisciplinary investigation of fundamental ridge-related problems on scales ranging from mantle convection to microbe activity. By accomplishing the goals of our proposal, our work will broadly impact a wide-range of scientific disciplines.

Development of human resources in the form of graduate and undergraduate student training is an important outgrowth of this proposal. Dunn and Wiens will incorporate undergraduate interns in various aspects of the work. These students will gather and analyze data and will be introduced to seismic imaging methods. Students will be chosen from through the IRIS, NSF or other education and outreach programs. Many of the students that will be involved represent groups that are historically underrepresented in science. For example, most U. of Hawaii undergraduates are residents of Hawaii and represent an ethnically diverse student body (19% Caucasian, 9% Filipino, 11% Native Hawaiian, 23% Japanese, 38% mixed or other), and most of the seismology graduate students at Washington University are female. It is intended that the laboratory and scholarly activities of each of the PIs will deepen the participation of these underrepresented groups in earth science. We will also work with Liz Goehring at the RIDGE office on outreach programs for K-12 and the general public. The Ridge office arranged for a science writer to work with the initial Lau cruises and we would seek continuing participation by her or another writer on our cruise, and seek to maintain a web site of ongoing Lau R2K activities.

This project will strengthen scientific ties to the kingdom of Tonga and will help raise that nationís scientific capabilities. Washington University has a long-standing collaborative relationship with the Ministry of Lands, Survey, and Natural Resources of Tonga. Several Tongan scientists have traveled as observers on the LABATTS cruises, have visited Washington University in the past, and would be invited to join the proposed cruises. The kingdom of Tonga is currently installing a small seismic monitoring network and Washington University personnel will assist Tongan scientists in their cataloging of seismic activity in Tonga.

8. Results from Prior Support

D. A. Wiens *EAR-9219675, $317,451, 5/1/93-10/31/97, "A passive broadband seismic experiment for study of subduction zone and back-arc structure and tectonics in the S. Pacific"* OCE-931446, $147,979, 6/1/94-5/31/98, "Seismic study of the Lau back-arc spreading center and Tonga Island Arc using OBSs". These grants funded a two-year deployment of eleven broadband digital seismic stations in the Southwest Pacific (SPASE), and a coincident 90-day deployment of 30 ocean bottom seismographs in the Lau back-arc (LABATTS). Our group has published 16 peer-reviewed papers resulting from this project. Regional Waveform inversion suggests upper mantle velocity heterogeneity of up to 16%, with exceptionally slow seismic velocities in the backarc basins, extending to depths of at least 200 km [*Xu and Wiens*, 1997]. Seismic tomography clearly images a slab, and suggests that slow velocity anomalies extend to depths of 400 km beneath the backarc spreading center [*Zhao et al*, 1997]. The ratios of S to P anomalies in the backarc are consistent with that expected for thermal anomalies but suggest only very limited presence of partial melt [*Koper et al*., 1999]. Attenuation tomography shows a low Q zone beneath the Lau spreading center [*Roth et al*, 1999a]. Comparison of attenuation and velocity tomographic images provides an empirical relationship between δV and δQ that is consistent with lab results [*Roth et al*., 2000]. Shear wave splitting results indicate a complex pattern of mantle flow in the Lau backarc, including inflow beneath the backarc from the north [*Smith et al*., 2001]. The large 1994 deep earthquake shows that the mainshock rupture zone and aftershocks can extend outside the active Benioff zone [*Wiens et al*., 1994; *Wiens* 2001].

R. A. Dunn OCE-01-17715; $92,121; 09/01/01-8/31/03; *Collaborative Research: Constraining mantle flow, melt supply, and lower crustal structure between the Clipperton and Siqueiros Fracture Zones from a seismic undershoot experiment.* (R. Dunn, R. Detrick; D. Toomey; W. Wilcock) The UNDERSHOOT experiment was designed to map the pattern of magma delivery from the mantle to the crust along the length of a transform-bounded segment of the East Pacific Rise. We found that at both crustal and mantle depth the EPR is underlain by a continuous low-velocity region. The results indicate that mantle flow and melt supply are broadly uniform along a section of ridge bounded by transform offsets. However, short wavelength variations (10-20 km scale) in the magnitude of the low-velocity zone suggest the presence of short-lived regions of enhanced melt flux into the crust [e.g., Nicholas et al., 1994]. We did not find evidence that OSCs reflect reductions in the underlying magma supply [*Dunn et al.,* 2001; *Christopher et al*., 2003; *Toomey et al*., 2003; *Jousselin et al*., 2003]. Other publications: *Dunn and Forsyth*, [2003]; *Cherkaoui et al*., [2003].

Donna K. Blackman, OCE-9812560 9/98-8/00, $93,54, Project Title: *Constructing a comprehensive seismological model of the EPR near the MELT experiment* (co-PIs D. Forsyth & D. Toomey). We developed of self-consistent flow and texturing models to explain observed seismic velocity and anisotropy patterns in the MELT EPR experiment. Texturing methodologies, effects of recrystallization, and influence of 3-D flow were tested, and a series of EPR models were investigated. We confirmed that some models could be ruled out. We illustrated cases where finite strain estimates of anisotropy do/don't match more complete estimates from polycrystal texturing [*Blackman et al*., 2002a; 2002b].

Spahr C. Webb, Spahr C. Webb and Wayne C. Crawford, OCE-9819159, *Measuring Crustal and Moho Melt Beneath the EPR, 910 N, Using Seafloor Compliance,* $282,088. The compliance technique detects regions of low shear modulus and data collected along the EPR [*Crawford and Webb*, 2002] reveal an asymmetric lower crustal melt zone beneath the axis between 9˚ and 10˚N comparable in width to that inferred from seismic tomography. The zone shifts west of the rise axis as the rise approaches the westward-stepping 9˚03'N OSC and is anomalously wide at the northern tip of the discontinuity. The measurements reveal a lower crustal melt zone 10 km off axis that is isolated from the axial melt body These Moho melt lenses are found at several locations both on and off-axis. The results suggests that the mantle melt supply controls the existence and location of crustal melt, but crustal processes provide the final control on the size and shape of the lower crustal melt zone.

William Menke, OCE-11965; $304,958; 08/15/98-11/30/00; *Active Seismic Imaging of Axial Volcano*; W. Menke & M. Tolstoy. Axial Volcano and the Juan de Fuca Ridge provide an excellent opportunity to study the interplay between active "hot spot" and "mid-ocean ridge" magmatic systems. The purpose of this research was to investigate the interconnectedness (or interaction) between these systems through the tomographic imaging of the region using seismic data from an active seismic airgun-to-obs experiment. The key elements of the new three-dimensional P-wave velocity model of the Axial and Coaxial magma systems are: 1. A large Axial magma chamber; A smaller Coaxial Magma Chamber, unconnected with the one at Axial; 3. Several small low velocity zones are possibly outlier magma chambers from Axial; 4. Thickening of the crust beneath Axial. The crust thickens from about 6 km far from Axial to 8 km near Axial to 11 km beneath the summit [*West*, 2001].